A&A 639, L13 (2020)
https://doi.org/10.1051/0004-6361/202038269

Astronomy & Astrophysics

LETTER TO THE EDITOR

Gas, dust, and star formation in the positive AGN feedback candidate 4C 41.17 at $z = 3.8$[⋆,⋆⋆]

N. P. H. Nesvadba[1], G. V. Bicknell[2], D. Mukherjee[3], and A. Y. Wagner[4]

[1] Université de la Côte d'Azur, Observatoire de la Côte d'Azur, CNRS, Laboratoire Lagrange, Bd de l'Observatoire, CS 34229, 06304 Nice Cedex 4, France
e-mail: nicole.nesvadba@oca.eu
[2] Research School of Astronomy and Astrophysics, The Australian National University, Canberra, ACT 2611, Australia
[3] Inter-University Centre for Astronomy and Astrophysics, Post Bag 4, Pune 411007, India
[4] University of Tsukuba, Center for Computational Sciences, Tennodai 1-1-1, 305-0006 Tsukuba, Ibaraki, Japan

Received 26 April 2020 / Accepted 28 May 2020

ABSTRACT

We present new, spatially resolved [CI]1–0, [CI]2–1, CO(7–6), and dust continuum observations of 4C 41.17 at $z = 3.8$. This is one of the best-studied radio galaxies in this epoch and is arguably the best candidate of jet-triggered star formation at high redshift currently known in the literature. 4C 41.17 shows a narrow ridge of dust continuum extending over 15 kpc near the radio jet axis. Line emission is found within the galaxy in the region with signatures of positive feedback. Using the [CI]1–0 line as a molecular gas tracer, and multifrequency observations of the far-infrared dust heated by star formation, we find a total gas mass of $7.6 \times 10^{10}\,M_{\odot}$, which is somewhat greater than that previously found from CO(4–3). The gas mass surface density of $10^3\,M_{\odot}\,\mathrm{yr}^{-1}\,\mathrm{pc}^{-2}$ and the star formation rate surface density of $10\,M_{\odot}\,\mathrm{yr}^{-1}\,\mathrm{kpc}^{-2}$ were derived over the 12 kpc × 8 kpc area, where signatures of positive feedback have previously been found. These densities are comparable to those in other populations of massive, dusty star-forming galaxies in this redshift range, suggesting that the jet does not currently enhance the efficiency with which stars form from the gas. This is consistent with expectations from simulations, whereby radio jets may facilitate the onset of star formation in galaxies without boosting its efficiency over longer timescales, in particular after the jet has broken out of the interstellar medium, as is the case in 4C 41.17.

Key words. galaxies: active – galaxies: high-redshift – galaxies: individual: 4C 41.17 – galaxies: jets – galaxies: star formation

1. Introduction

It is now widely recognized that powerful radio jets ejected by powerful active galactic nuclei (AGN) can have a major impact on the evolution of their host galaxies by regulating their gas content and interstellar medium conditions, thereby potentially facilitating the formation of new stars. Outflows of molecular, atomic, and warm ionized gas found in numerous galaxies are our prime observational evidence of feedback today.

Other potential mechanisms, by which the injection of AGN energy may regulate star formation in the host galaxies, are much less explored. This includes the enhancement of gas turbulence and pressure within the interstellar gas and star-forming clouds. A pressure increase on embedded gas clouds may temporarily facilitate star formation ("positive feedback"; e.g., Fragile et al. 2004, 2017; Wagner et al. 2012; Silk 2013). The existence of such positive feedback has been expected theoretically for several decades, but observational evidence is hard to collect, and is only found for very few individual targets in the nearby and distant universe (Croft et al. 2006; Salomé et al. 2015, 2017). Maiolino et al. (2017) suggest that velocity offsets found in a nearby ultraluminous infrared galaxy (ULIRG) may also point to positive feedback associated with radio-quiet quasar activity.

An interesting question is whether positive feedback can boost the efficiency with which stars form from molecular gas beyond the levels found in intensely star-forming galaxies, as postulated by some models of galaxy evolution (Gaibler et al. 2012; Silk 2013; Mukherjee et al. 2018). Shocks driven into the gas by the radio jet may compress the denser regions of these clouds and lead to star formation from gas that was previously marginally Jeans-stable (e.g., Wagner et al. 2012; Fragile et al. 2017). The rare candidates at low redshift with signatures of positive feedback often seem to fall below the relationship between molecular gas mass and star formation rate density, suggesting these galaxies form stars at lower efficiency than those without AGN (Salomé et al. 2017). However, our clearest examples of positive feedback in the nearby Universe are either dwarf galaxies (e.g., Minkowski's Object, 3C 285, Salomé et al. 2015) or the outskirts of massive early-type galaxies (e.g., Cen A, Salomé et al. 2017). These examples have low gas-mass surface densities compared to actively star-forming galaxies, and therefore they do not allow us to infer whether or not AGN may boost star formation in environments dominated by dense molecular gas. Mukherjee et al. (2018) found from relativistic hydrodynamic simulations that the efficiency of star formation in such galaxies likely depends strongly on the detailed properties of the gas clouds, jet power, and interaction geometry, making it very

⋆ IRAM data are only available at the CDS via anonymous ftp to cdsarc.u-strasbg.fr (130.79.128.5) or via http://cdsarc.u-strasbg.fr/viz-bin/cat/J/A+A/639/L13
⋆⋆ Based on data obtained with the IRAM NOEMA interferometer through program S19DA.

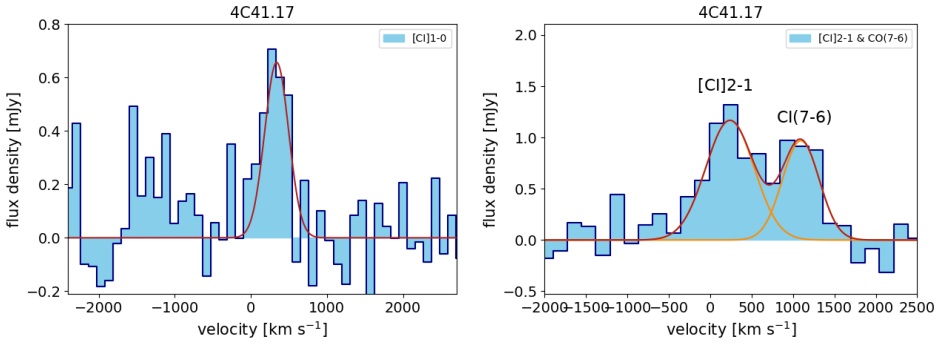

Fig. 1. Integrated spectra of [CI]1–0 (*left*), and the [CI]2–1 and CO(7–6) lines (*right*). The red and orange lines show the total fit to the line profile and the fits to the individual components, respectively.

difficult to predict theoretically whether the net effect of the radio jet on star formation is positive or negative.

To test whether positive feedback may enhance the star formation efficiency in massive galaxies in the early Universe, we observed the powerful radio galaxy 4C 41.17 at $z = 3.792$ (Chambers et al. 1990) with the NOEMA interferometer of the Institut de Radioastronomie Millimetrique (IRAM), probing the [CI] lines of atomic carbon and the dust continuum at ∼500 GHz rest-frame frequency. We observed [CI] rather than CO because this line is the more reliable tracer of molecular gas mass at high redshift, it is optically thin, and is less affected by gas excitation effects than the more commonly observed mid-J CO lines (e.g., Papadopoulos & Greve 2004; Valentino et al. 2018; Nesvadba et al. 2019). 4C 41.17 is arguably our best example of positive AGN feedback in the early Universe, as shown by the alignment of extended, unpolarized Lyα emission with the radio jet axis (Dey et al. 1997), strongly kinematically perturbed gas (Steinbring 2014), and asymmetric absorption-emission spectra typical of very young stellar populations (P Cygni profiles; Dey et al. 1997). Bicknell et al. (2000) present a detailed analytical study of the potential gas compression by the radio jet, finding that at least parts of the extended Lyα emission associated with the radio jet axis and bright extended UV continuum may originate from star formation in gas compressed through the passage of the radio jet. A young starburst age of 30 Myr is also supported by multicomponent SED fitting (Rocca-Volmerange et al. 2013) and is consistent with the age estimate of the radio jet (Bicknell et al. 2000).

In the following we describe our observations of the gas, dust, and star formation in 4C 41.17, and discuss our results in the light of star formation in massive galaxies at high redshift with and without radio jets. We use the flat ΛCDM cosmology from Planck Collaboration VI (2020) with $H_0 = 67.4\,\mathrm{km\,s^{-1}\,Mpc^{-1}}$, $\Omega_\mathrm{M} = 0.315$, and $\Omega_\Lambda = 1-\Omega_\mathrm{M}$. At $z = 3.792$ the luminosity distance is $D_\mathrm{L} = 34.41$ Gpc, and 7.26 kpc are projected onto one arcsecond.

2. NOEMA interferometry of 4C 41.17

4C 41.17 was observed between June and December 2019 with the NOEMA interferometer in the 2 mm and 3 mm bands with either 9 or 10 antennae in the C configuration under average to good atmospheric conditions. The central frequencies were 102.705 and 168.895 GHz, respectively, corresponding to the observed frequencies of [CI]1–0 and [CI]2–1 at $z = 3.79198$, respectively. The source was observed for a total of 7.0 h and 5.6 h in the 2 mm and 3 mm bands, respectively. The data were calibrated with the Continuum and Line Interferometer Calibration package CLIC[1] and with MWC349 and LKHA101 as flux calibrators. Combining both polarizations leads to a continuum root mean square (rms) of 7.3 μJy bm^{-1} and 23.9 μJy bm^{-1} in the 3 mm and 2 mm bands, respectively, measured over 3.8 GHz bandwidth. We rebinned the data to a spectral resolution of 20 MHz in both bands (corresponding to 58 km s^{-1} in band 3, and 36 km s^{-1} in band 2, respectively), and obtained a line rms of 0.1 and 0.3 mJy bm^{-1} and per spectral channel, respectively. With natural weighting, we obtain a beam size of $2.3'' \times 1.7''$, and $1.4'' \times 1.0''$ at 3 mm and 2 mm, respectively. Figure 1 shows the resulting integrated spectra.

Table 1. Observational results.

Line	Velocity [km s^{-1}]	*FWHM* [km s^{-1}]	I_line [Jy km s^{-1}]	S_cont [mJy]
[CI]1–0	228 ± 21	372 ± 21	0.26 ± 0.03	0.11 ± 0.015
[CI]2–1	237 ± 52	686 ± 56	0.84 ± 0.07	0.49 ± 0.035
CO(7–6)	95 ± 55	526 ± 56	0.53 ± 0.06	0.49 ± 0.035

Notes. Velocities are given relative to $z = 3.792$.

Figure 2 shows the [CI] and dust morphology. All line emission is concentrated within an area of full width at half maximum (FWHM) $2.8'' \times 1.7''$ around the radio core for [CI]1–0, and $1.8'' \times 1.1''$ for the [CI]2–1 and CO(7–6) lines, respectively. The major axis of the line emission exceeds the major axis size of the beam significantly in both bands, clearly showing that the emission is resolved along this axis, but not extended enough to neglect beam smearing. Gaussian deconvolution suggests major axis lengths of $1.6''$ and $1.3''$ for the [CI]1–0 and the [CI]2–1 and CO(7–6) lines, respectively.

The continuum, best seen in the 2 mm band, is strongly elongated and more extended along the major axis than the line emission observed in the same band, has an observed size of $2.4'' \times 1.1''$, and a deconvolved size of $2.0''$. For simplicity, and because our main goal is to rule out that the star formation rate surface density exceeds those measured in other galaxies, we adopt a common size of $1.6'' \times 1.1''$ for the area emitting [CI]1–0 and the dust continuum.

The continuum major axis is roughly aligned with the radio jet axis. Integrated continuum flux densities, which are measured after subtracting the line emission from the data cubes, are 488 ± 24 and 112 ± 7 μJy in the 2 mm and 3 mm band, respectively. Integrated line and continuum fluxes are listed in Table 1. As already noted by De Breuck et al. (2005), the nonthermal synchrotron emission from the radio source does not significantly change these measurements.

To extract line fluxes, we fit the [CI]1–0 line with a single Gaussian centered on a velocity of (228 ± 21) km s^{-1} relative to $z = 3.97197$, a FWHM line width of (372 ± 21) km s^{-1} and a flux of $I_\mathrm{CI10} = (0.26 \pm 0.03)$ Jy km s^{-1}.

[1] http://www.iram.fr/IRAMFR/GILDAS

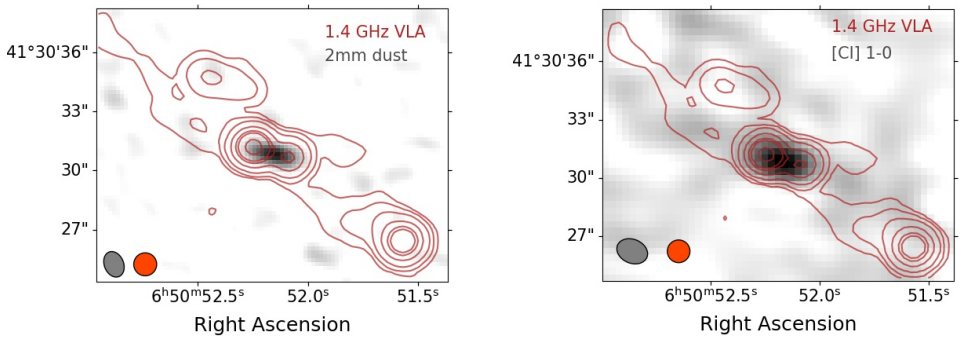

Fig. 2. Dust (*left*) and [CI]1–0 morphology (*right*) of 4C41.17. Contours show the 1.4 GHz radio morphology. The radio core is between the two central components (Bicknell et al. 2000). The beam size is shown in the lower left corner of each panel.

A two-component fit to the [CI]2–1 and CO(7–6) lines yields integrated line fluxes of $0.84 \pm 0.07\,\mathrm{Jy\,km\,s^{-1}}$ for [CI]2–1, and $0.53 \pm 0.06\,\mathrm{Jy\,km\,s^{-1}}$ for CO(7–6), respectively. Both lines are significantly broader than the [CI]1–0 line: CO(7–6) has $FWHM = 527 \pm 56\,\mathrm{km\,s^{-1}}$, whereas [CI]2–1 has $FWHM = 686 \pm 56\,\mathrm{km\,s^{-1}}$. It is possible that [CI]2–1 and CO(7–6) luminosities are enhanced near the AGN relative to [CI]1–0, since both probe relatively high-excitation gas. The ratio $R_{21/10} = 3.2$ of [CI]1–0 and [CI]2–1 flux falls near the divide between gas heated by AGN and star formation, but into the star formation regime (Meijerink et al. 2007). It is therefore possible that parts of the [CI]2–1 emission are from gas heated by the AGN. It is also interesting to note that we do not see the same double-peaked line profile in CO(7–6) that De Breuck et al. (2005) previously found for CO(4–3), which may also indicate differences in gas excitation.

3. Gas and star formation properties

We used Eq. (4) of Alaghband-Zadeh et al. (2013), $M_{\mathrm{H_2,[CI]}} = 1380 \times \frac{D_\mathrm{L}^2}{(1+z)}\, A_{10,-7}^{-1}\, X_{\mathrm{CI},-5}^{-1}\, Q_{10}^{-1}\, I_\mathrm{CI}\,[M_\odot]$, where D_L is the luminosity distance in units of Gpc, z the redshift, I_CI the integrated line flux of [CI]1–0 in $\mathrm{Jy\,km\,s^{-1}}$. The Einstein A coefficient, $A_{10} = 7.93 \times 10^{-8}$ is given in units of $10^{-7}\,\mathrm{s^{-1}}$, and the carbon abundance, $X_\mathrm{CI} = 3 \times 10^{-5}$ (Alaghband-Zadeh et al. 2013), in units of 10^{-5}. We find a molecular gas mass of $M_\mathrm{H2} = (7.6 \pm 1.0) \times 10^{10}\,M_\odot$, which is somewhat greater than the $5.4 \times 10^{10}\,M_\odot$ previously found by De Breuck et al. (2005) from CO(4–3) with a $7'' \times 5''$ beam; this is a sufficient to cover most of the surrounding Lyα halo. This suggests that we have not resolved more extended line emission associated with 4C 41.17.

We estimated the star formation rates from the dust continuum in the NOEMA data at 2 mm and 3 mm and used previous *Herschel*/SPIRE and ground-based single-dish measurements taken from the compilation of Drouart et al. (2014) to determine the dust temperature, T_D and the β parameter. We only used observations taken at $\geq 350\,\mu$m, where the AGN contamination is <5% in the spectral energy distribution (SED) of dust shown by Drouart et al. (2014). This suggests $T_\mathrm{D} = (53 \pm 3)\,\mathrm{K}$ and $\beta = 1.9$, respectively, for a modified blackbody fit calculated in the same way as in Canameras et al. (2015). This SED overpredicts the observed flux densities by factors 2.5 and 2 in the 2 mm and 3 mm bands, respectively (Table 1). This may either be due to missing flux in the interferometry data or additional, fainter dust emission within the much larger beam size (10–20″) of the single-dish observations. A potential candidate for additional far-infrared (FIR) emission would be diffuse emission from the large, $5'' \times 7''$, Lyα halo previously found by van Breugel et al. (1999). In the following we use the fluxes obtained with NOEMA, which are best matched to the [CI] emission-line region rather than those derived from the single-dish measurements.

We adopted a modified version of the relationship of Kennicutt (1998a) to estimate a star formation rate from the FIR luminosity. Using the Chabrier stellar initial mass function this implies $\mathrm{SFR}\,[M_\odot\,\mathrm{yr^{-1}}] = 2.5 \times 10^{-44}\,L_\mathrm{FIR}\,[\mathrm{erg\,s^{-1}}]$. We find a total star formation rate of $\mathrm{SFR} = 650\,M_\odot\,\mathrm{yr^{-1}}$. This is a factor ~2 greater than the $\mathrm{SFR} = 290\,M_\odot\,\mathrm{yr^{-1}}$ of star formation that van Breugel et al. (1999) found for the UV continuum in the same region, which is likely affected by dust extinction. Averaged over a region of $1.6'' \times 1.1''$ (11.6 kpc × 8 kpc at $z = 3.79$), this corresponds to star formation and gas mass surface densities of $\Sigma_\mathrm{SFR} = 8.9\,M_\odot\,\mathrm{yr^{-1}\,kpc^{-2}}$ and $1040\,M_\odot\,\mathrm{yr^{-1}\,pc^{-2}}$, respectively. Since we measured and resolved [CI] and the dust continuum with similar beam sizes, these results are robust, even if some of the discrepancy between the continuum measurements with NOEMA and single-dish telescopes should be due to missing flux instead of additional astrophysical sources.

4. Discussion and summary

Gas mass and star formation rate surface density in galaxies are closely related; they have a near-linear relationship that holds over more than six orders of magnitude in star formation and for molecular gas mass surface densities $>10\,M_\odot\,\mathrm{pc^{-2}}$ (e.g., Kennicutt 1998b; Bigiel et al. 2008). Actively star-forming galaxies at high redshift tend to fall above that relationship, as first noted by Daddi et al. (2010) and Genzel et al. (2010), indicating shorter gas consumption times and potentially higher star formation efficiency.

Figure 3 shows where 4C 41.17 falls in this Schmidt-Kennicutt diagram between star formation and gas mass surface density, averaged over the 11.6 kpc × 8 kpc area previously defined in Sect. 2, and the gas mass and star formation rate from Sect. 3. We also add the second galaxy with potential evidence of jet-triggered star formation in the early Universe, PKS 0529−549 at $z = 2.6$, to this analysis. This galaxy was previously discussed by Man et al. (2019), who point out that star formation in this source seems to be more efficient than in giant molecular clouds in the Milky Way. Both galaxies fall well above the typical relationship found for disk galaxies in this redshift range, which are on the main sequence of star formation, as already noted by Man et al. (2019). However, the star formation rates do not fall above those found in other intensely star-forming galaxies at the same cosmic epoch (Bothwell et al. 2010), which likely include the progenitors of powerful high-redshift radio galaxies.

This result suggests that the star formation efficiency does not exceed that found in other strongly star-forming galaxies without AGN, at least when averaged over the ~10 kpc regions where jet-triggered star formation was found (Dey et al. 1997). We might

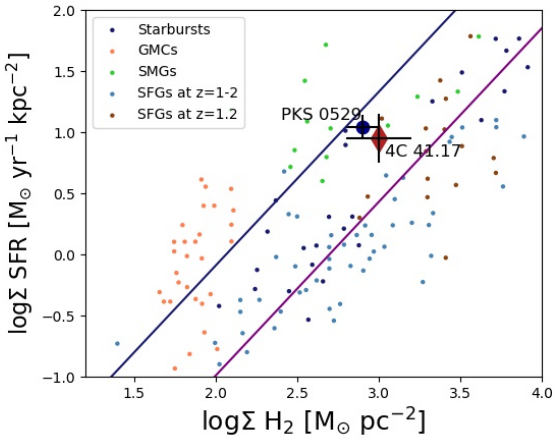

Fig. 3. Gas and star formation rate surface densities of 4C 41.17 (red diamond), PKS 0529−549 (blue dot), and several comparison samples: Giant molecular clouds in the Milky Way (Evans et al. 2014), local starburst galaxies (Kennicutt 1998a), star-forming galaxies at $z = 1$–2 (Tacconi et al. 2008; Valentino et al. 2018, 2020), and submillimeter galaxies (Bothwell et al. 2010). The solid purple and blue lines indicate the sequences for typical main-sequence and starburst galaxies of Daddi et al. (2010).

suspect that positive and negative feedback would both be present and partially cancel the effect on each other (Dugan et al. 2017; Mukherjee et al. 2018). Steinbring (2014) found outflow signatures in warm ionized gas in 4C 41.17, suggesting that negative feedback is at work, although the low line width of [CI]1–0 does not suggest that a large percentage of the cold neutral gas is currently being removed. However, in situ gas removal through winds would also lower the observed gas-mass surface densities. This would move the galaxy to the left in Fig. 3 and artificially enhance, not lower, the observed star formation efficiency.

A more likely explanation is that the phase of positive feedback is very short and only triggers the onset of star formation without boosting it over longer timescales. This is not unexpected from a theoretical point of view: initial hydrodynamic simulations suggested that jet-triggered star formation may be long-lived (Gaibler et al. 2012), but did not take into account energy and momentum losses through disk porosity. More recent work suggests that the impact of the jet on the star formation drops after a short initial "kick-off" phase (Fragile et al. 2017; Mukherjee et al. 2018). This would also be consistent with the very high star formation rates of 7300 $M_\odot\,\mathrm{yr}^{-1}$ required to form the $2.2 \times 10^{11}\,M_\odot$ of young stars found by Rocca-Volmerange et al. (2013) within 30 Myr, that is, an order of magnitude higher than today. Figure 2 also shows that the jet has already broken out of 4C 41.17, suggesting it may no longer be able to sustain a high overpressure within the gas. Jet-triggered star formation may also be limited by star formation itself once the starburst has evolved past the first few million years, as previously suggested by Fragile et al. (2017). At 30 Myr age (Rocca-Volmerange et al. 2013), the starburst in 4C 41.17 is clearly evolved enough to have produced the first generations of supernovae. These may make star formation in 4C 41.17 self-regulating, as has previously been suggested for other massive, intensely star-forming galaxies at $z = 2$–3 (e.g., Lehnert et al. 2013).

To summarize, we used new [CI]1–0 and 2–1, CO, and dust continuum interferometry obtained with IRAM/NOEMA to study star formation in 4C 41.17 at $z = 3.8$, which is the best example of positive feedback from radio jets at high redshift in the literature. We estimated a molecular gas mass of $7.6 \times 10^{10}\,M_\odot$ in an elongated region where signatures of jet-triggered star formation have previously been found. The spatially resolved gas and star formation rate densities suggest that stars are formed at efficiencies that are comparable to submillimeter galaxies at the same epoch. The same is true for PKS 0529−549, the second galaxy with likely signatures of a very young, potentially jet-triggered, stellar population.

While our results do not call into question the previous good evidence for jet-triggered star formation in 4C 41.17 obtained in the UV and radio, they do suggest that this phase is very short and not sustained after the jet has broken out from the interstellar gas of the host galaxy. After few 10 Myr, jet-triggered star formation proceeds with similar efficiency as in other intensely star-forming galaxies, making the signatures of positive feedback difficult to identify observationally. This result is also consistent with recent observational and theoretical findings in low-redshift galaxies, which indicate that jet-triggered star formation does not necessarily lead to a boost in star formation efficiency, even at high gas-mass surface densities of up to 1000 $M_\odot\,\mathrm{pc}^{-2}$.

Acknowledgements. We thank the referee for having gone through our Letter carefully, and for comments which helped clarify some aspects of our analysis. We also thank the IRAM staff, in particular Charlène Lefèvre, for taking these data, and their excellent support with the data reduction.

References

Alaghband-Zadeh, S., Chapman, S. C., Swinbank, A. M., et al. 2013, MNRAS, 435, 1493
Bicknell, G. V., Sutherland, R. S., van Breugel, W. J. M., et al. 2000, ApJ, 540, 678
Bigiel, F., Leroy, A., Walter, F., et al. 2008, AJ, 136, 2846
Bothwell, M. S., Chapman, S. C., Tacconi, L., et al. 2010, MNRAS, 405, 219
Canameras, R., Nesvadba, N., Guery, D., et al. 2015, MNRAS, 362, 41
Chambers, K. C., Miley, G. K., & van Breugel, W. J. M. 1990, ApJ, 363, 21
Croft, S., van Breugel, W., de Vries, W., et al. 2006, ApJ, 647, 1040
Daddi, E., Elbaz, D., Walter, F., et al. 2010, ApJ, 714, L118
De Breuck, C., Downes, D., Neri, R., et al. 2005, A&A, 430, L1
Dey, A., van Breugel, W., Vacca, W. D., & Antonucci, R. 1997, ApJ, 490, 698
Drouart, G., De Breuck, C., Vernet, J., et al. 2014, A&A, 566, A53
Dugan, Z., Gaibler, V., Bieri, R., Silk, J., & Rahman, M. 2017, ApJ, 839, 103
Evans, N. J., II, Heiderman, A., & Vutisalchavakul, N. 2014, ApJ, 782, 114
Fragile, P. C., Murray, S. D., Anninos, P., & van Breugel, W. 2004, ApJ, 604, 74
Fragile, P. C., Anninos, P., Croft, S., Lacy, M., & Witry, J. W. L. 2017, ApJ, 850, 171
Gaibler, V., Khochfar, S., Krause, M., & Silk, J. 2012, MNRAS, 425, 438
Genzel, R., Tacconi, L. J., Gracia-Carpio, J., et al. 2010, MNRAS, 407, 2091
Kennicutt, R. C., Jr. 1998a, ARA&A, 36, 189
Kennicutt, R. C., Jr. 1998b, ApJ, 498, 541
Lehnert, M. D., Le Tiran, L., Nesvadba, N. P. H., et al. 2013, A&A, 555, A72
Maiolino, R., Russell, H. R., Fabian, A. C., et al. 2017, Nature, 544, 202
Man, A. W. S., Lehnert, M. D., Vernet, J. D. R., De Breuck, C., & Falkendal, T. 2019, A&A, 624, A81
Meijerink, R., Spaans, M., & Israel, F. P. 2007, A&A, 461, 793
Mukherjee, D., Bicknell, G. V., Wagner, A. E. Y., Sutherland, R. S., & Silk, J. 2018, MNRAS, 479, 5544
Nesvadba, N. P. H., Cañameras, R., Kneissl, R., et al. 2019, A&A, 624, A23
Papadopoulos, P. P., & Greve, T. R. 2004, ApJ, 615, L29
Planck Collaboration VI. 2020, A&A, in press https://doi.org/10.1051/0004-6361/201833910
Rocca-Volmerange, B., Drouart, G., De Breuck, C., et al. 2013, ArXiv e-prints [arXiv:1301.1983]
Salomé, Q., Salomé, P., & Combes, F. 2015, A&A, 574, A34
Salomé, Q., Salomé, P., Miville-Deschênes, M. A., Combes, F., & Hamer, S. 2017, A&A, 608, A98
Silk, J. 2013, ApJ, 772, 112
Steinbring, E. 2014, AJ, 148, 10
Tacconi, L. J., Genzel, R., Smail, I., et al. 2008, ApJ, 680, 246
Valentino, F., Magdis, G. E., Daddi, E., et al. 2018, ApJ, 869, 27
Valentino, F., Magdis, G. E., Daddi, E., et al. 2020, ApJ, 890, 24
van Breugel, W., Stanford, A., Dey, A., et al. 1999, in The Most Distant Radio Galaxies, eds. H. J. A. Röttgering, P. N. Best, & M. D. Lehnert, 49
Wagner, A. Y., Bicknell, G. V., & Umemura, M. 2012, ApJ, 757, 136